F80/82: Scintillators and Coincidence Spectrometers

Fortgeschrittenen Praktikum,

18.08.2025 - 19.08.2025

Participants: **Jonathan Rodemers, Maria Susdorf**

Contents

1. F80: Scintillators

1.1 Signal of the scintillator

The setup of this part of the experiment was done according to the provided manual (see [3], page 20). The resulting signals with and without the Cs-137 source were observed and sketched, with and without amplifying the signal. By slowly increasing the voltage and observing its effects, a value of 447 V was decided to be suitable for further measurements.

For signals without a source, only noise has been detected. Since this signal is (ideally) very weak, the amplifier had a negligible effect on its strength. For the two signals with the Cs-137 source, a clear minimum was observed for both measurements. However, an additional extremum (a maximum), was only visible by amplifying the Cs-137 signal.

Thus, for measurements without the amplifier, obtaining a truly meaningful signal was not possible, since information could be lost. It was also shown that measurements without a source wouldn't produce a signal resembling that of a source, even with the amplifier. This meant that false signals due to calibration errors of the setup were unlikely. The signal of the measurement with the amplifier *and* the Cs-137 source provided a "stable" signal, that is, the oscilloscope triggered fast enough to make it appear to be constant. A sketch of the observed pulse can be seen in figure 1.1.

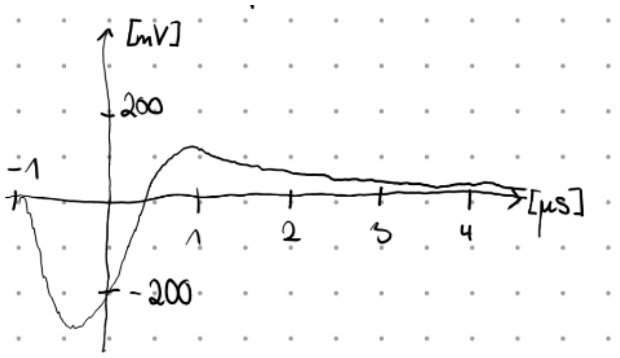

Figure 1.1: Sketch of amplified signal with Cs-137 source

1.2 Measuring and understanding the pulse height spectrum

To be able to complete the rest of this experiment, it is important to understand the pulse height spectrum. For this, a voltage of 447 V, as determined in the previous section, was chosen. The energy spectrum of the Cs-137 source was captured using the NaI scintillator, an amplifier and an ADC that was connected to a PC, where the data was recorded.

The information about the energy level of a signal is encoded in its pulse height, which in turn is encoded in an ADC channel number. Since both the total gain and the amplification of the setup affect the pulse height, the position of the peaks (i.e. at which channel numbers they appear) can be adjusted by varying them. Since the ADC has a limited channel range, and the channels correspond to different energy levels, this is necessary to ensure that most of the ADC channel range was being used without saturating it. There were a total of 1024 ADC channels available (after binning), which meant a recording with a differentiation between 1024 different energy level ranges was possible.

Additionally, to avoid recording too many counts at low energy levels, which are not caused by the source, a threshold value can be set. This is because binning very low energy background noise together

with the range corresponding to energies below that of the second ADC channel would significantly increase the recorded counts in the first ADC channel.

By trial and error, a gain of 32 and a threshold value of 8200 were determined to capture a usable spectrum of the Cs-137 source, as seen in figure 1.2.

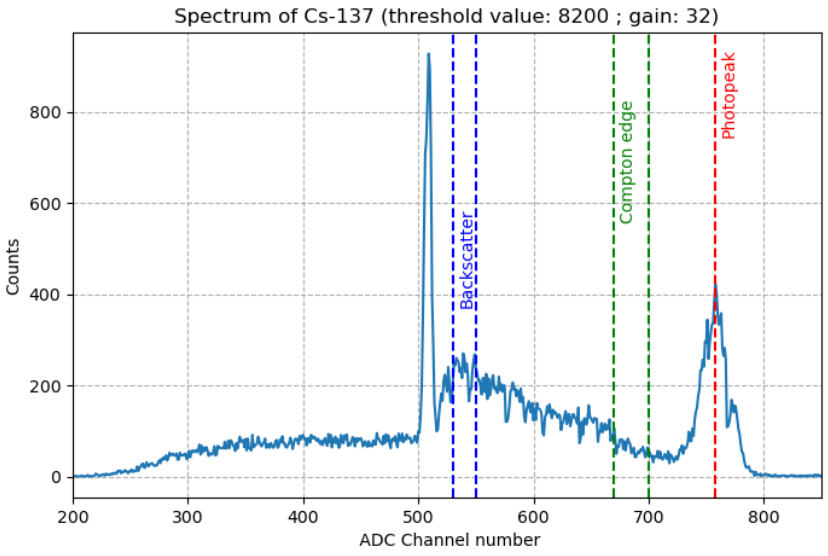

Figure 1.2: Captured Cs-137 spectrum with labeled identified structures.

The structure on the right, which lies at channel 756 ± 3, was easily identified to be the photo peak of caesium. The structure in the middle, in the channel range of about 520 to 700, depicts the Compton continuum. The tall peak on the left is very likely to appear due to the decay of Ba-137m, which is also part of the decay process of Cs-137 with a probability of 94.7 %. This isotope decays through γ-radiation, so with a distinct energy, as seen in the sharpness of the peak. Ba-137 itself is stable, so decay of this isotope should not be present in the data.

Furthermore, the Compton edge and the back-scatter peak in the continuum were able to be identified, as seen in figure 1.2.

1.3 Pulse height as a function of voltage

The voltage that was previously set to 447 V is the total operating voltage of the photomultiplier in the scintillator setup. This means the voltage also sets the gain factor of the photomultiplier itself, with the following correlation:

$$G = (kV)^N \tag{1.1}$$

where G is the photomultiplier's gain, k is a proportionality factor, V is the voltage in MeV and N is the number of stages of the multiplier.

Thus, the curve of the Pulse Height–Voltage plot was expected to resemble a polynomial. Since the exact number of stages inside the multiplier was unknown, a more precise prediction of the curve was not possible.

Recording the position of the photo peak of Cs-137 at various voltages led to the following results:

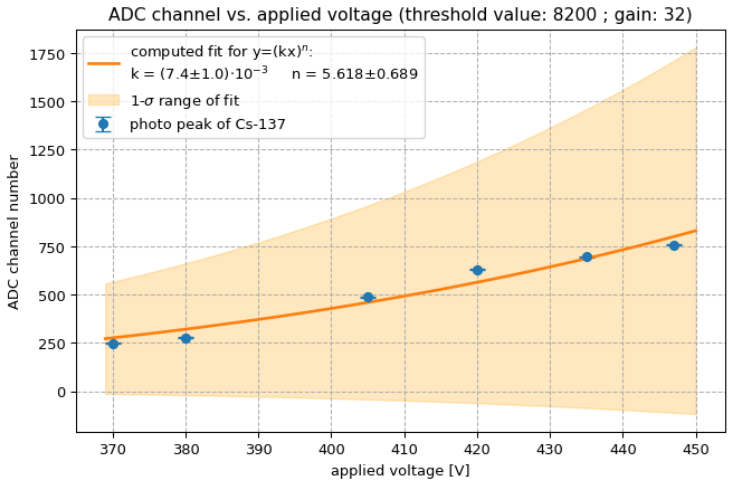

Figure 1.3: Applied voltage vs. photo peak position

A clean polynomial fit with only one term (of the N-th degree) was unable to be determined. However, the best fit (with a reduced χ^2-value of 272.049) using the method of least squares was determined to be:

$$G = (kV)^N = (7.352 \cdot 10^{-3}\ V)^{5.618}$$

This would imply a non-integer value for N, which doesn't make sense in the context of counting the number of stages of the photo multiplier. An explanation of this could be the fact that this model only considers the ideal case. There are additional losses to be considered, which would affect the exponent, making it smaller than the theoretical value. In reality, the efficiency ϵ of a photo multiplier stage is not represented by an integer ($0 < \epsilon < 1$), which would explain why the computed exponent usually isn't an integer either ($\Rightarrow \text{avg}(\epsilon) \cdot N_{\text{stages}}$).

1.4 Choosing a working voltage

The goal of choosing a working voltage was to achieve the highest possible resolution of the measured spectrum. For this, the energy of the photo peak of ^{137}Cs , E, and its FWHM, ΔE, were used to compute the relative error, $\Delta E/E$. In this case, using the ADC channel numbers instead of energy is equivalent, since they are proportional, with proportionality factors canceling out. The lowest relative error corresponds to the highest resolution.

Voltage [V]	450	440	430	420	410
ΔE / E	5.4 %	6.2 %	6.6 %	6.9 %	6.2 %

Table 1.1: Voltage vs. relative error

Since the lowest error was achieved at 450 V, this voltage was used for all further measurements.

1.5 Energy calibration

Since the ADC channel number has been used to compare the positions of different peaks up until now, the next goal is to determine the factor used to convert ADC channel numbers to their respective

MeV values. This calibration was done using Co-60 and Cs-137 as sources with known energy levels, followed by fitting a linear function to the data that correlates the ADC channel numbers and the MeV values of the peaks.

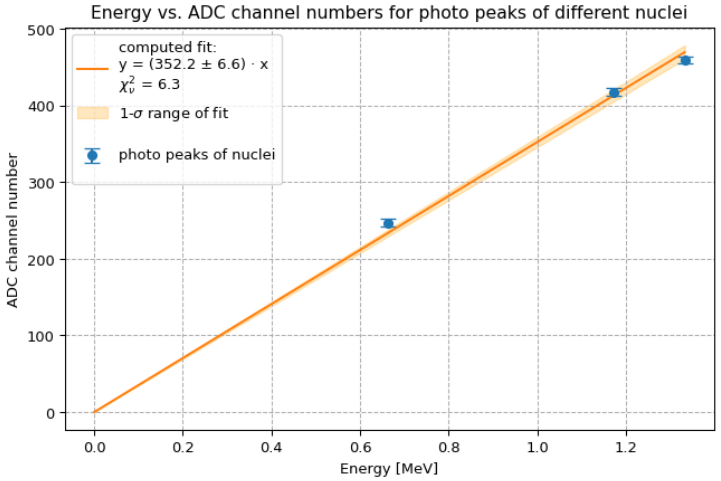

Figure 1.4: Energy calibration fit (ADC channel number to MeV)

The proportionality factor in this case was determined to be $k = 352.2 \pm 6.6$ and will be used to convert energy in MeV to corresponding ADC channel numbers.

1.6 Determination of the end-point energy via Kurie plot

To determine the endpoint energy of the Sr-90 source, two methods were used. First, the spectrum of the Sr-90 source was measured. Then, acrylic glass was introduced to the setup, which blocked the radiation of Sr-90 and thus served as a background measurement. This was subtracted from the Sr-90 spectrum. Then, the linear region of the continuum was identified and a linear fit was computed. The endpoint energy was determined by extrapolating to the point at which the Kurie-value should be zero, according to the computed fit.

The endpoint energy obtained with this method was

$$E_{0,\text{acrylic}} = (2.011 \pm 0.089)\ \text{MeV}$$

Comparison to values from literature makes this more likely to be the endpoint energy of Y-90 decay, not Sr-90.

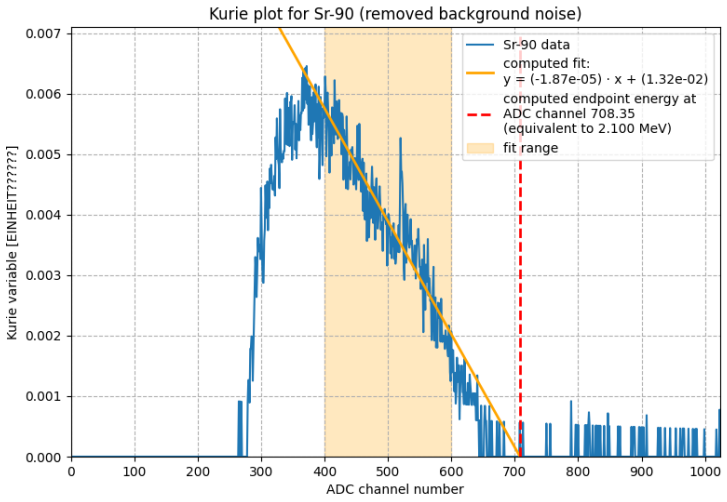

Figure 1.5: Corrected Sr-90 spectrum with linear fit

The second method involved placing aluminum sheets of different thicknesses in the path of the β-radiation of the source. Therefore, the endpoint energies can be evaluated individually and then extrapolated to "zero aluminum thickness". This was also done using the linear region of the continuum for a linear fit and determining the point where the count should be zero.

This method provided a different, but similar result for the endpoint energy:

$$E_{0,\text{aluminum}} = (1.763 \pm 0.584)\ \text{MeV}$$

Due to essentially describing the same physics, this value is also more likely to be the endpoint energy of Y-90 decay, just as the previous method did.

The plot depicting the extrapolation can be seen below:

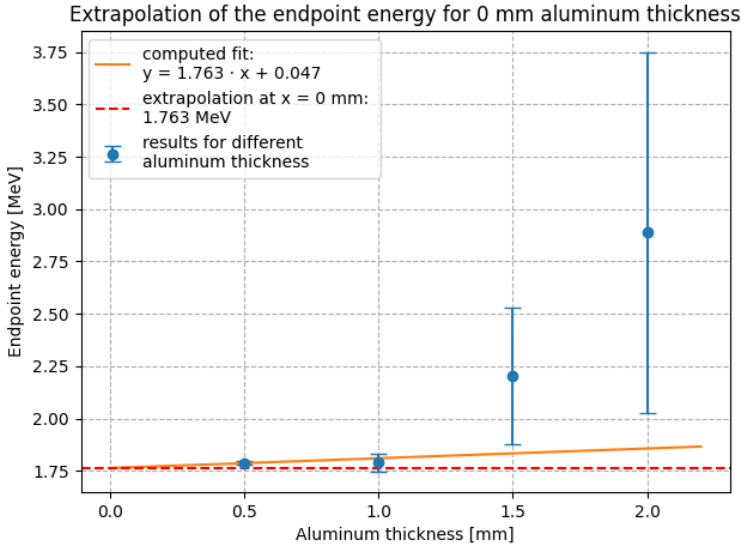

Figure 1.6: Endpoint energies with a weighted linear fit.

2. F82: Coincidence Spectrometers

2.1 Material and Methods

2.1.1 Setting up Electronics

The experiment was set up according to the manual's instructions (see [2], page 8). The cables were labeled to remember which position corresponds to what signal seen on the oscilloscope.

To only select pulses within the desired height range, a "Timing Single Channel Analyzer" - or more briefly, a "TSCA" - was used.

After setting it up, a pulse of constant height (with fluctuations due to the technical limitations of a digital signal) was detected in the second channel only when the first channel's signal was above a certain threshold level set by the TSCA.

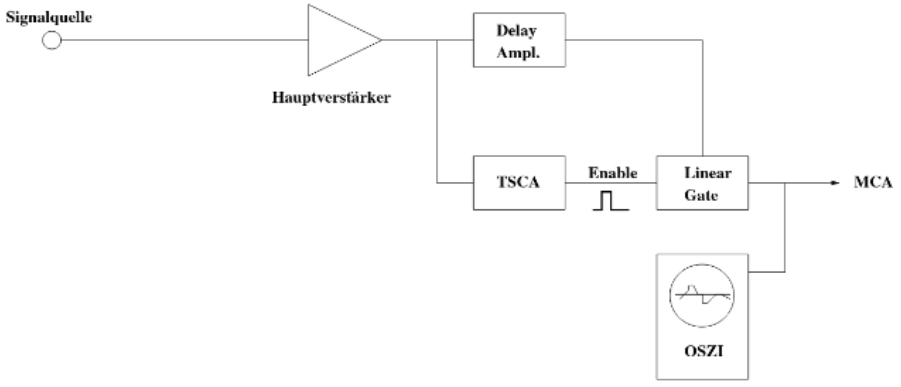

Figure 2.1: Schematic diagram of circuit used. (taken from F82 manual [2], unchanged)

To use a linear gate with the TSCA, the signal is split so that the TSCA and a delay amplifier receive the same signal. Since the TSCA itself has an inevitable delay, the delay for the amplifier is needed. Just like before, the TSCA only sends a rectangular pulse which either enables (opens) or disables (closes) the gate for the duration of the pulse. For the delay amplifier, the goal is to set a suitable delay time to ensure the digital signal from the TSCA and the analog signal reach the linear gate at the same time.

Using this circuit, the specific range of signals to observe can be selected, since the gate only opens when the signal itself is within a range set by adjusting the "upper" and "lower" potentiometer settings.

After setting up the linear gate, a sketch of the resulting signal using a delay time of 1.75 μs was created:

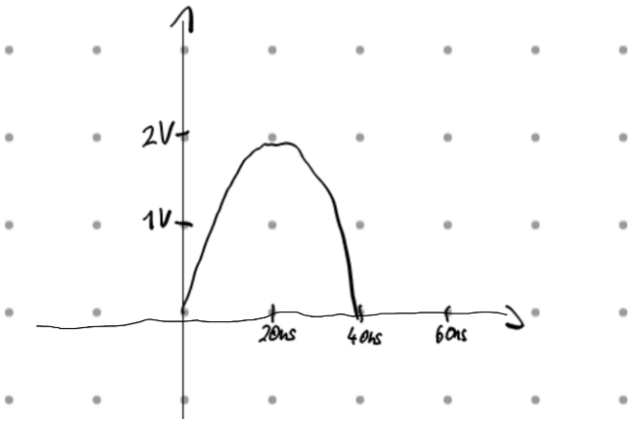

Figure 2.2: Sketch of the observed signal.

2.1.2 γ-Spectra of Different Radionuclei

To calibrate the setup, the spectra of nuclei with known peak positions were measured. In this experiment, Cs-137, Co-60, Na-22 and Ba-133 sources were used for this purpose. The individual measurements were stopped once all relevant structures were visible. A threshold value of 15 was determined to be acceptable.

To ensure all energy levels of the relevant structures were visible for all samples, the Cs-137 sample was observed first, due to its relatively high activity resulting in a clearly visible peak. Since the ratio between energy levels is the same as the ratio between their corresponding ADC channels, the position of the Cs-137 peak was set so the highest expected energy peak (i. e. from Co-60) would still be visible with the given range of ADC channels.

2.2 Results

2.2.1 γ-Spectra of Different Radionuclei

An overview of the relevant range of every spectrum taken is given below:

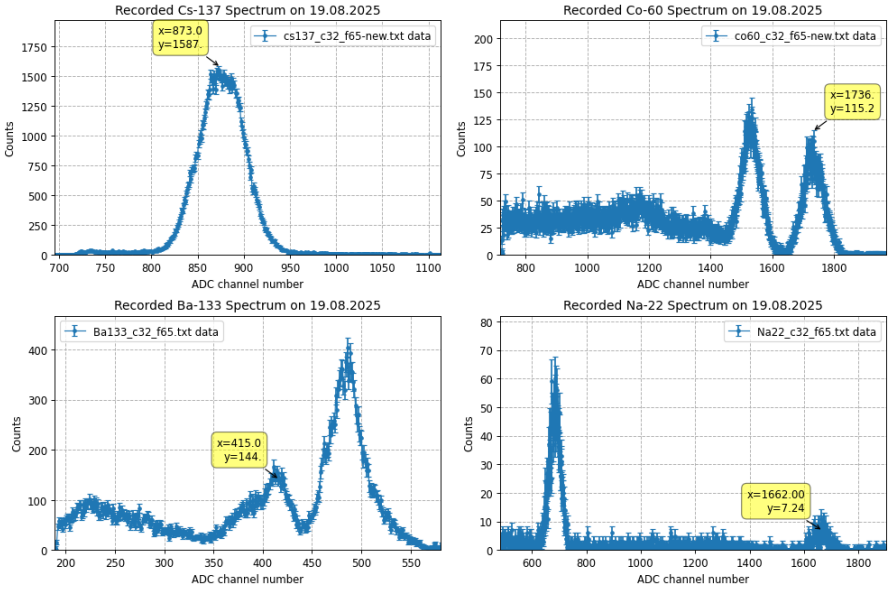

Figure 2.3: Overview of the spectra taken.

2.2.2 Energy Calibration and Resolution

For a quantitative measurement, a calibration has to be completed. This was done using the known photo peak energies for all samples and considering annihilation peaks. By identifying the ADC channels at which the peaks appear and matching them to the expected energies, the proportionality factor can again be computed using a linear fit. This returned a proportionality factor of $k = 1307.9 \pm 5.3$.

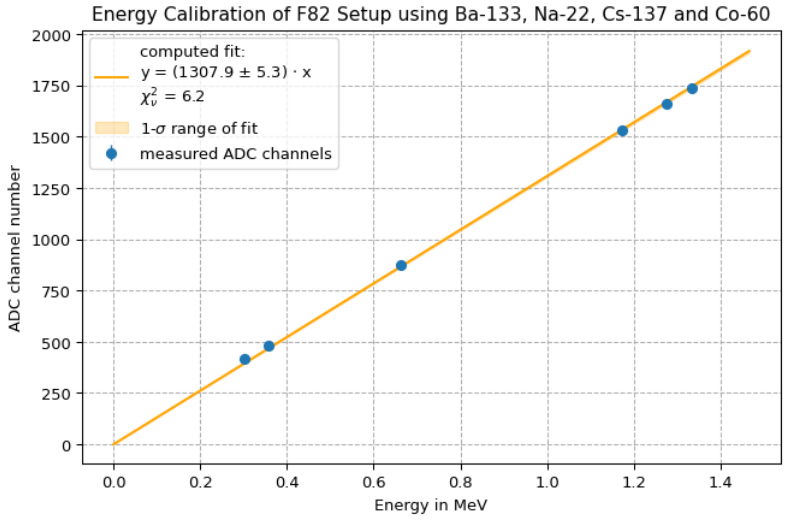

Figure 2.4: Linear fit for the energy calibration of the F82 setup.

Furthermore, it is now possible to evaluate the different energy resolutions for different peaks, $\Delta E/E$. As for the value of ΔE, the FWHM values of the peaks were again obtained using python code that computed a Gaussian fit for each peak. The following figure shows this process for the Cs-137 photo peak as an example.

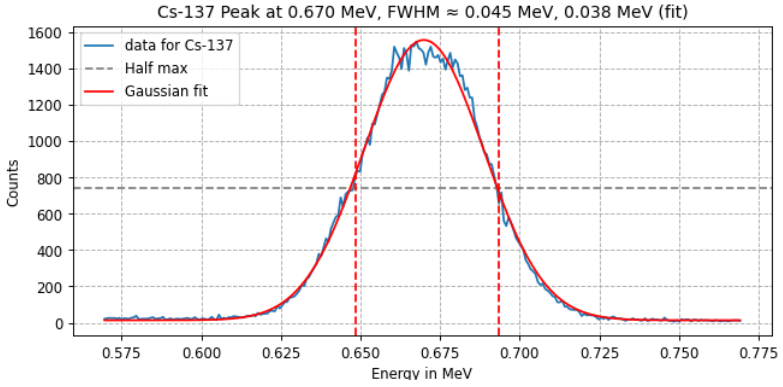

Figure 2.5: Example of Gaussian Fit for FWHM estimation of Cs-137 Peak

The results of this method can be seen in the table below:

Peak	FWHM [MeV]	E [MeV]	ΔE/E
Cs-137	0.038	0.670	5.65 %
Co-60 (left peak)	0.049	1.168	4.18 %
Co-60 (right peak)	0.054	1.325	4.09 %
Na-22	0.046	1.275	3.60 %
Ba-133 (left peak)	0.018	0.316	5.67 %
Ba-133 (right peak)	0.021	0.372	5.74 %
Error	0.004	0.003	0.31 %

Table 2.1: FWHM, energy and energy resolution for all measured peaks.

To compare these values, the peak's energy, E, was plotted against its resolution, $\Delta E/E$.

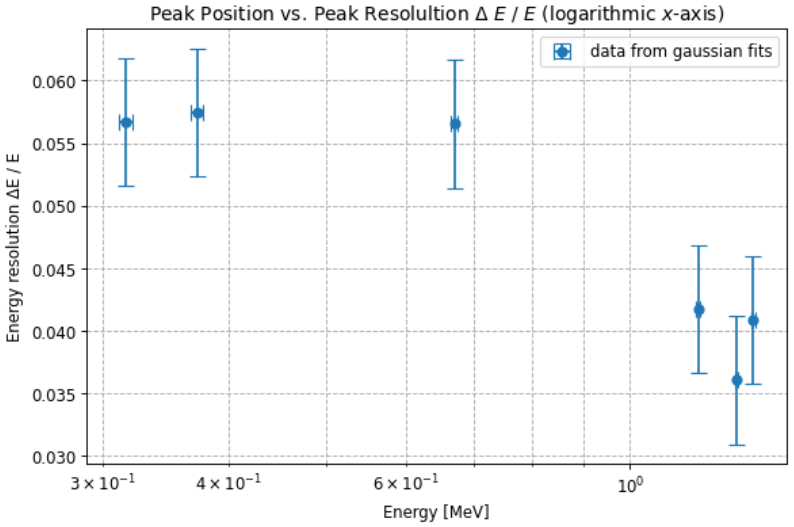

Figure 2.6: Energy vs. Resolution of Different Nuclei Peaks with Logarithmic x-axis.

The relative energy resolution $\Delta E/E$ improves (i. e. decreases) with higher energies because of the statistical nature of the scintillation process. The number of scintillation photons produced is proportional to the deposited energy E, while the statistical fluctuations scale with the square root of the number of photons, assuming a Poisson distribution.

$$\frac{\Delta E}{E} = \frac{\sqrt{E}}{E} = \frac{1}{\sqrt{E}}$$

2.2.3 Spectra

All spectra appeared to have peaks at energies below 100 keV. As they are not the result of the sources themselves, they will only be mentioned in the discussion.

2.2.3.1 Cs-137

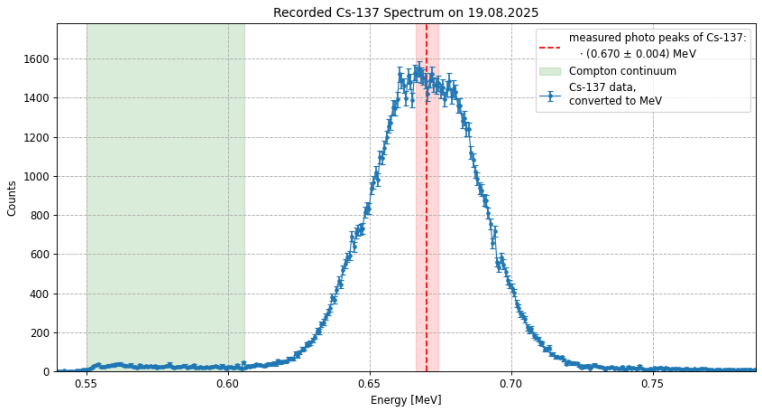

Figure 2.7: Analysis of Cs-137 Spectrum

As shown in the plot above, a photo peak at (0.670 ± 0.004) MeV and the Compton continuum to the left of it were able to be identified. The Compton continuum signal is a lot weaker than the photo peak signal, so it can't be identified easily in this zoomed-out version of this plot, but this was only done to allow the photo peak of Cs-137 to appear in full height.

2.2.3.2 Co-60

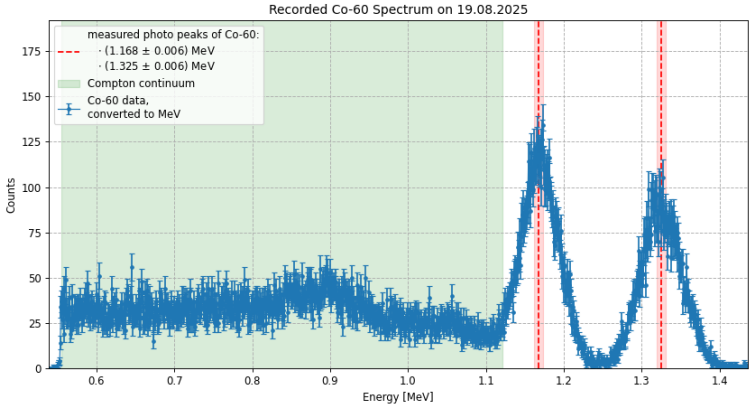

Figure 2.8: Analysis of Co-60 Spectrum

The photo peaks at (1.168 ± 0.006) MeV and (1.325 ± 0.006) MeV, as well as the Compton continuum, were easily identifiable. However, the Compton edges were unable to be determined due to the signal not appearing clearly enough.

2.2.3.3 Na-22

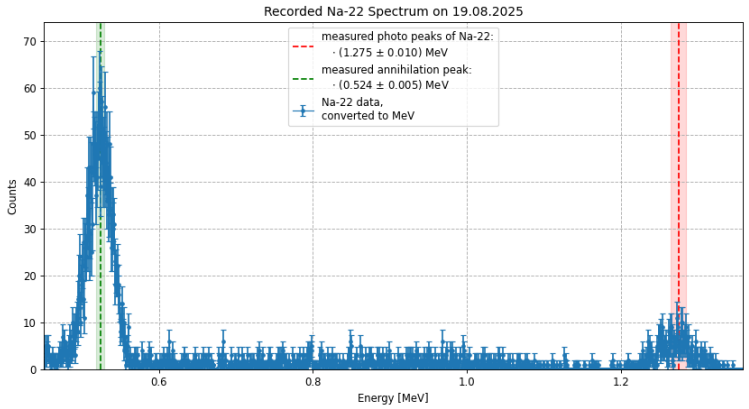

Figure 2.9: Analysis of the Na-22 Spectrum

The (524 ± 5) keV line observed in the spectrum is highly likely to be the electron-positron annihilation peak and provides direct evidence of positron emission and pair annihilation. The peak seen to the right of it, at (1.275 ± 0.010) MeV, is the photo peak of the Na-22 spectrum.

2.2.3.4 Ba-133

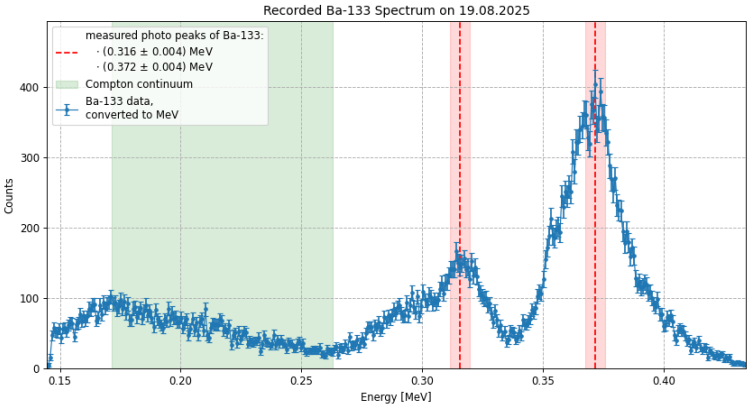

Figure 2.10: Analysis of Ba-133 Spectrum

Again, the photo peaks and the Compton continuum were able to be identified. The photo peaks of Ba-133 were determined to lie at (0.316 ± 0.004) MeV and (0.372 ± 0.004) MeV.

2.2.4 Night Measurement

Since it was recommended to compare the overnight background radiation spectrum to that of the isotope K-40, the energy of the γ-decay of Ar-40*, a product of K-40 decay, was marked in the following plot according to it's literature value (see [1]). The expected 511 keV from electron-positron annihilation was marked as well.

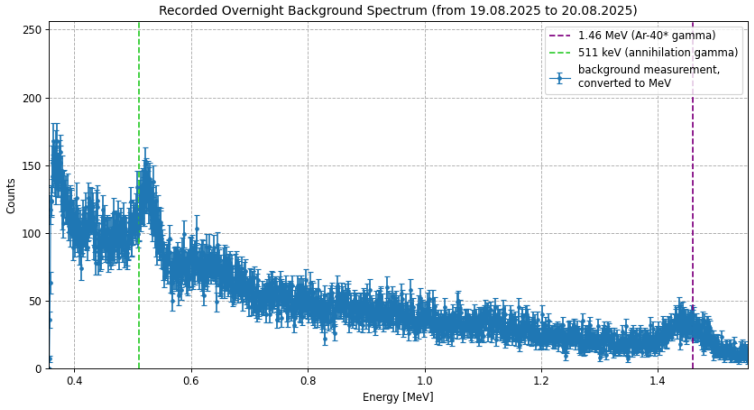

Figure 2.11: Analysis of Overnight Background Spectrum

The energy from the γ-radiation of Ar-40* matches the recorded peak at (1.445 ± 0.011) MeV reasonably well. The peak at around (524 ± 9) keV is also close to the energy of electron-positron annihilation, meaning it has likely occurred even without a source as well.

Bumps in the presumed Compton continuum seen throughout the entire plot may be due to other commonly found isotopes causing background radiation or the conditions inside the lab.

The comparison with the K-40 spectrum lead to the conclusion that there may be K-40 present in the earth's mantle, which is confirmed by online research. The annihilation peak is likely to be the result of β^+-decay, which is also part of a decay branch of K-40.

Contact with K-40 is incredibly common, even being contained inside bananas. It is the largest source of natural radioactivity in animals, including humans. [1]

3. Discussion

3.1 F80: Scintillators

3.1.1 Number of Stages inside of the Photo Multiplier

The best fit for applied voltage vs. ADC channel number computed that $N = 5.618 \pm 0.690$.

This would imply a non-integer value for N, which doesn't make sense in the context of counting the number of stages of the photo multiplier. An explanation of this could be the fact that this model only considers the ideal case. There are additional losses to be considered, which would affect the exponent, making it smaller than the theoretical value. In reality, the efficiency ϵ of a photo multiplier stage is not represented by an integer ($0 < \epsilon < 1$), which would explain why the computed exponent usually isn't an integer either. $\Rightarrow \text{avg}(\epsilon) \cdot N_{\text{stages}}$

3.1.2 Endpoint Energy

The method involving the Kurie-variable provided a fairly accurate result. The uncertainty was very likely to be underestimated, since only inaccuracies of the computed fit according to python were considered. However, this method only used one measurement only.

The aluminum method used four measurements, but had a much higher uncertainty for its result, (1.763 ± 0.584) MeV. As seen in figure 1.6, the data points for thicker layers of aluminum have very high relative errors. This implies that measurements for thicker layers should be longer to ensure a similar count as for thinner layers, making the fits to determine the endpoint energies at those thicknesses more accurate. It is also the reason why a weighted fit isn't close to the last two data points at all - their uncertainties were just too large, as is also seen in figure 1.6.

The difference in accuracy and precision of estimating the endpoint energy could be due to several factors. One of them could be the aforementioned larger statistical errors for thicker aluminum sheets.

3.2 F82: Coincidence Spectrometers

3.2.1 Unusual Structures at Lower and Highest ADC channel numbers

3.2.1.1 Spike in Highest ADC Channel

In the Co-60 and overnight spectra, the last ADC channel, number 2047, shows a sudden spike in counts. Since this doesn't appear in the channels right before it, this is very likely due signals of higher than about 1.565 MeV being recorded without being able to be displayed properly due to the limited range. Other spectra have not displayed a significantly higher count in the last channel. Since the Co-60 and overnight spectra are also the only ones that displayed an annihilation peak, this may imply a common cause connected to electron-positron annihilation.

3.2.1.2 Signals at Low Energies

As mentioned before, all spectra appeared to have peaks at energies below 100 keV. For energies below 100 keV, the spectra of the nuclei sources compare as follows:

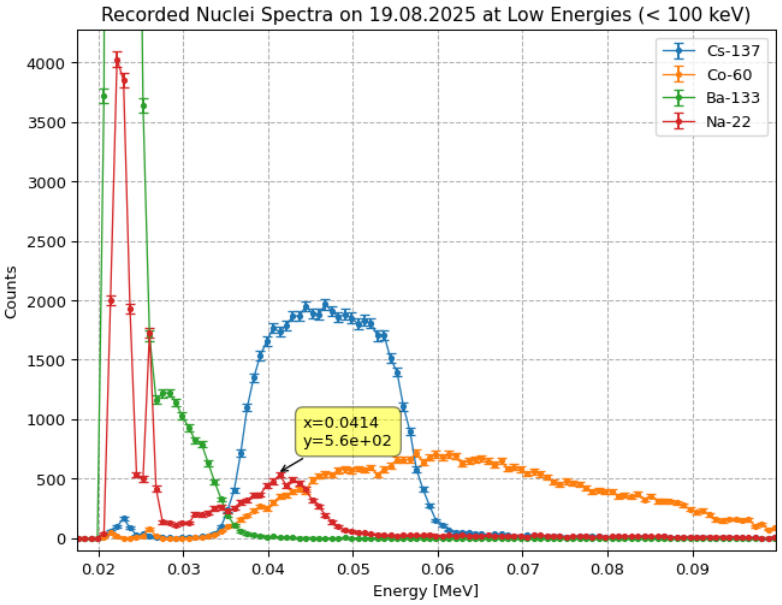

Figure 3.1: Data at lower end of available ADC channels, converted to MeV.

Possible causes include electronic noise or environmental gamma sources, especially when considering the lab has a lot of electronics inside of it and is probably slightly more radioactive than the average university building.

Cosmic radiation would also be a possible cause, since it can't really be excluded in this lab course.

Electrons transitions between energy levels inside an atom are also possible, which would explain why the low energy peaks appear to have different characteristics for different nuclei. Nuclide-specific interactions with its environment would have a similar effect.

Finally, γ-rays resulting from interactions inside the detector housing are likely, especially when considering that the TSCA should have filtered those signals before they could arrive at the detector. Therefore, their presence in the recorded spectra may indicate incomplete filtering or leakage of signal.

However, the overall spectra at low energies are most likely to be caused by several factors, including the ones mentioned, since the low-energy peaks have higher counts than the characteristic structures of the source they appear with.

4. Summary

In the first part of this report, F80/81, the first goal was to familiarize oneself with its setup. Characteristic structures were able to be identified. The effective number of stages inside the photomultiplier was determined to be $N = 5.618 \pm 0.689$. A working voltage was determined by opting for the highest energy resolution, after which an energy calibration was done using Co-60 and Cs-137 as sources. This allowed for the endpoint energy of Sr-90 to be determined using two methods. The Kurie plot provided a result of (2.011 ± 0.089) MeV, while using aluminum to extrapolate to "zero thickness" returned a result of 1.763 ± 0.584 MeV.

For the second part, F82/83, the workings behind the circuit of the setup were thoroughly explored. Spectra of different nuclei, namely Cs-137, Co-60, Na-22 and Ba-133, were recorded. Again, an energy calibration was done. The energy resolutions for different peaks were computed and compared to the energies of the peaks. The spectra were again analyzed using the computed conversion to MeV. The analysis of an overnight background measurement revealed that K-40 plays a significant role in the daily exposure of humans and animals to natural radiation. It was also revealed that electron-proton annihilation also happens often enough to be identified on such a spectrum, even without a source.

Bibliography

[1] *Potassium-40*. Wikipedia, the free encyclopedia https://en.wikipedia.org/wiki/Potassium-40. – [Last access: 15.10.2025]

[2] Universität Heidelberg: *F82/83: Koinzidenzspektrometer*. https://www.physi.uni-heidelberg.de/Einrichtungen/FP/anleitungen/F82.pdf. Version: 2015. – [Last access: 19.08.2025]

[3] Universität Heidelberg: *F80/F81: Scintillators*. https://www.physi.uni-heidelberg.de/Einrichtungen/FP/anleitungen/F80.pdf. Version: 2018. – [Last access: 18.08.2025]